Journal of Geophysical Research: Solid Earth

Supporting Information for

Postseismic deformation following the 2015 Mw7.8 Gorkha (Nepal) earthquake: new GPS data, kinematic and dynamic models, and the roles of afterslip and viscoelastic relaxation

J. Liu-Zeng[1,2], Z. Zhang[3], C. Rollins[4,5*], A. Gualandi,[5,6], J.-P. Avouac[5], H. Shi[7], P. Wang[1], W. Chen[8], R. Zhang[7], P. Zhang[1], W. Wang[1], Y. Li[7], T. Wang[7] and Z. Li[1]

1. State Key Laboratory of Earthquake Dynamics, Institute of Geology, China Earthquake Administration, Beijing, China
2. Institute of Surface Earth System Science, Tianjin University, Tianjin, China
3. Institute of Tibetan Plateau Research, Chinese Academy of Sciences, Beijing, China
4. School of Earth and Environment, University of Leeds, UK
5. Division of Geological and Planetary Sci., California Institute of Technology, Pasadena, CA, USA.
6. Jet Propulsion Laboratory, California Institute of Technology, Pasadena, CA, USA.
7. China Earthquake Networks Center, Beijing, China
8. Department Research Center of China Earthquake Administration, Beijing, China

*j.c.rollins@leeds.ac.uk

Contents of this file

S1. Notes on GPS processing and data preparation

We process the raw GPS data using GAMIT/GLOBK [Herring et al., 2015]. We first obtain a regional fiducial free solution under relaxed constraints for the joint synchronous data together with 10 stable IGS stations in the surrounding region (KIT3, LHAZ, POL2, URUM, KUNM, TASH, GUAO, ULAB, HYDE, IISC). The geophysical model and method used are kept consistent with the seven global subnet solutions provided by IGS (IGS 1-7; ftp://garner.ucsd.edu/pub/). Next, we combine the regional solution and the IGS solutions into one daily solution at the normal equation level by common parameters. We then obtain the conversion parameters relative to ITRF2008 [Altamimi et al., 2011] via a 7-parameter similarity transformation by including 80 uniformly distributed global GPS reference stations in the daily solution, and then these conversion parameters to convert the fiducial solutions to ITRF2008 (Figures 3-4, light gray). Our timeseries agree well with those from NGL at stations included in both datasets (figures in Liu_etal_ts_UNRcomparison.zip), except for spurious offsets that are sometimes not corrected in automatically processed time series. At these common stations the weighted root-mean-square difference between the two solutions is on average 2.6, 2.4, and 8 mm in the east, north, and vertical components, comparable to the mean nominal uncertainties of 3, 3, and 10 mm for the east, north, and vertical daily GPS positions.

In the timeseries processed here, station ODRE has missing data for more than 1 yr before the mainshock and an offset from an antenna change in 2013, complicating the estimation of interseismic motion, and so we use the NGL timeseries at this station, which is continuous from 2004. Stations KIRT, KOLH, NAST, TAPO and WAMR have large (>15 mm/yr) vertical rates that are likely nontectonic in origin; KIRT and NAST in particular are located in the Kathmandu basin and are likely affected by aquifer usage. We therefore do not include these five stations in the velocity fields that we interpolate to other stations by kriging; we do, however, use the India-relative trajectory-model velocities at KIRT and NAST for those stations individually, as this captures the fact that their rapid vertical motions are background rather than postseismic. The timeseries called LCK5 is a concatenation of those from stations LCK2 and LCK3, as LCK3's coverage started immediately after LCK2's stopped and they have nearly the same location. Likewise, the timeseries called LCK6 is a concatenation of those from stations LCK4 and LCKI.

In the vbICA analysis, we use the notation of Gualandi et al. [2017], where U and V have unit norm columns and the total displacement at each station is reproduced by multiplying U, V and S.

S2. Notes on the kinematic inversions and forward models

The preferred kinematic afterslip model (Figure 8a) features some shallow strike-slip afterslip that fits the vertical motions at KKN4, NAST and MKLU and the eastward motion at MKLU, but this slip is likely not real: KKN4 and NAST may be affected by anthropogenic motion and MKLU was inoperative during the early postseismic period and had an offset later that was corrected but may have introduced a bias.

In the forward models, we allow slip on the narrow region in between the mainshock and Mw7.3 aftershock (Figure 1a, brown region) by setting the low but nonzero slip in this region in the Elliott et al. [2016] models – which would otherwise contribute a stress drop there and prevent afterslip in stress-driven models – to zero. We also set slip to zero in the isolated low-slip region to the northwest of station CHLM [Elliott et al., 2016, fig. 1]. These changes have very little effect on the overall moment release.

S3. Estimation of elastic strain release from postseismic deformation and from aftershocks

We estimate a total postseismic strain release equivalent to a moment between $[1.21 \pm 0.15] \times 10^{20}$ Nm and $[2.37 \pm 0.13] \times 10^{20}$ Nm (Section 6). The upper bound was obtained by extrapolating the postseismic displacements to the origin time of the mainshock, using the preferred kinematic afterslip model (Figure 8a) and assuming an increase of shear modulus with depth from 30 GPa to 43 GPa in the zone of afterslip (Figure 9d). The lower bound ignores postseismic deformation over the first day, assumes a uniform shear modulus of 30 GPa, and is based on the afterslip model obtained with positivity constraints and pure dip slip motion as this is the one that yields the smallest slip potency (Figure S3c).

The estimate of 2.98×10^{19} Nm released in aftershocks (Figure 8a, black circles) includes the moment released by undetected small aftershocks, which is estimated by extrapolating the magnitude-frequency distribution below the detection threshold for unboundedly small earthquakes with an assumed b-value of 1 [Gualandi et al., 2017].

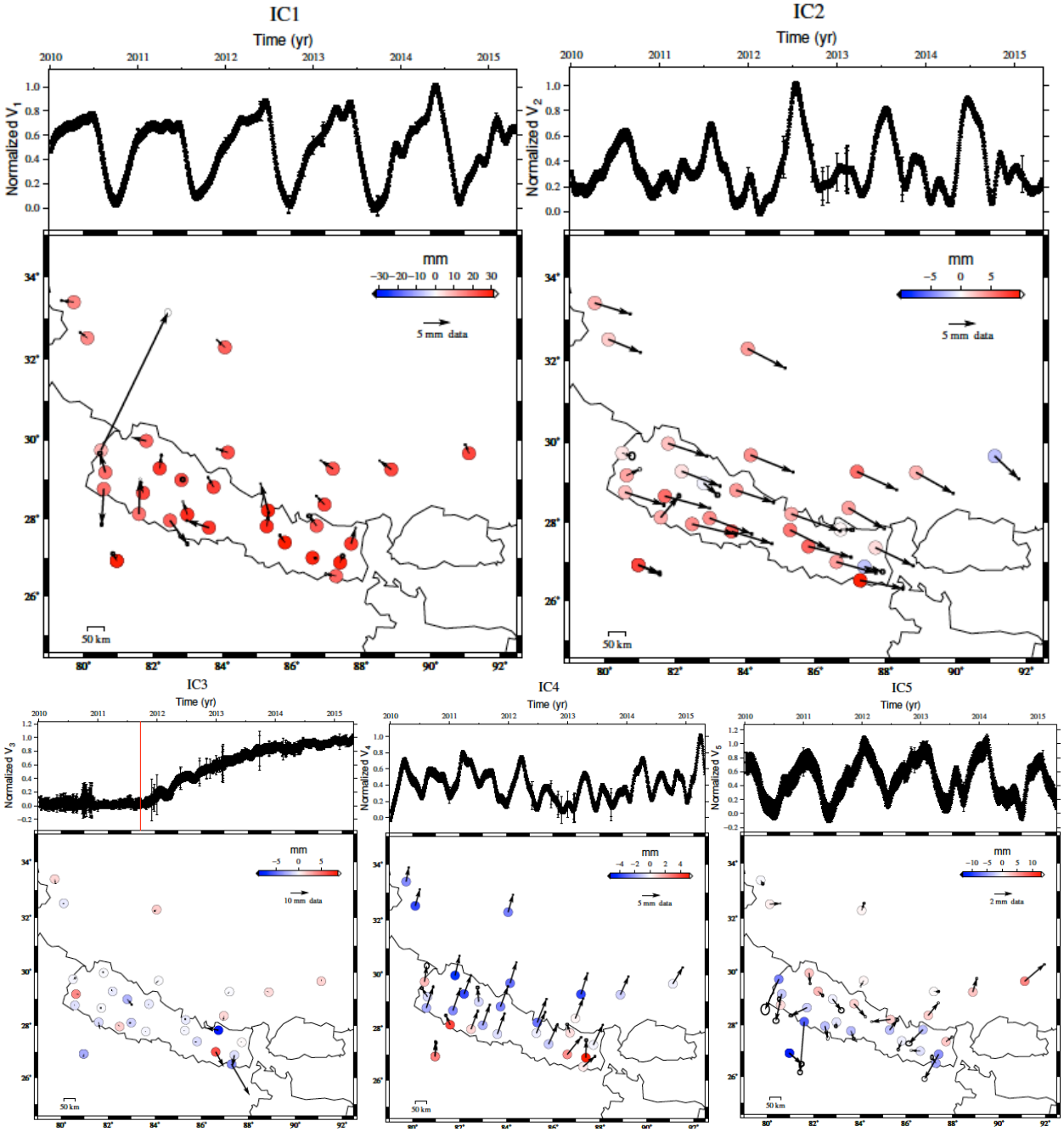

Fig. S1. Independent Components (ICs) for the preseismic time range (section 2): temporal components *V* (timeseries) and spatial components *U* (mapviews). The corresponding weights are 1664.7 mm, 597.0 mm, 468.0 mm, 399.9 mm and 392.0 mm, respectively. The red line in the timeseries of IC3 shows the time of the Sikkim earthquake (2011 September 18). The time series have been corrected for the co-seismic offset related to that earthquake, while the post-seismic deformation of that earthquake is isolated by this method (and subsequently removed).

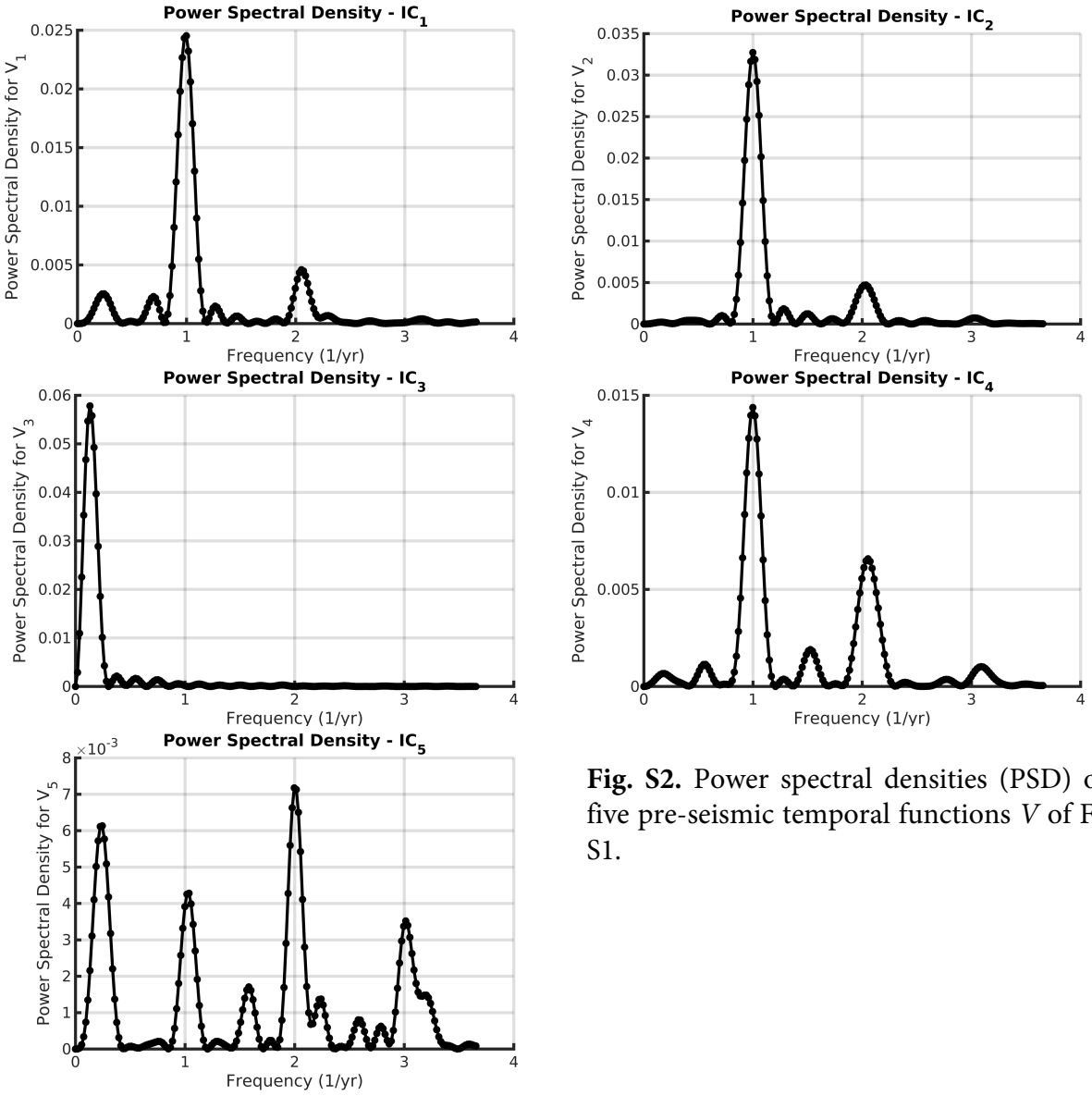

Fig. S2. Power spectral densities (PSD) of the five pre-seismic temporal functions *V* of Figure S1.

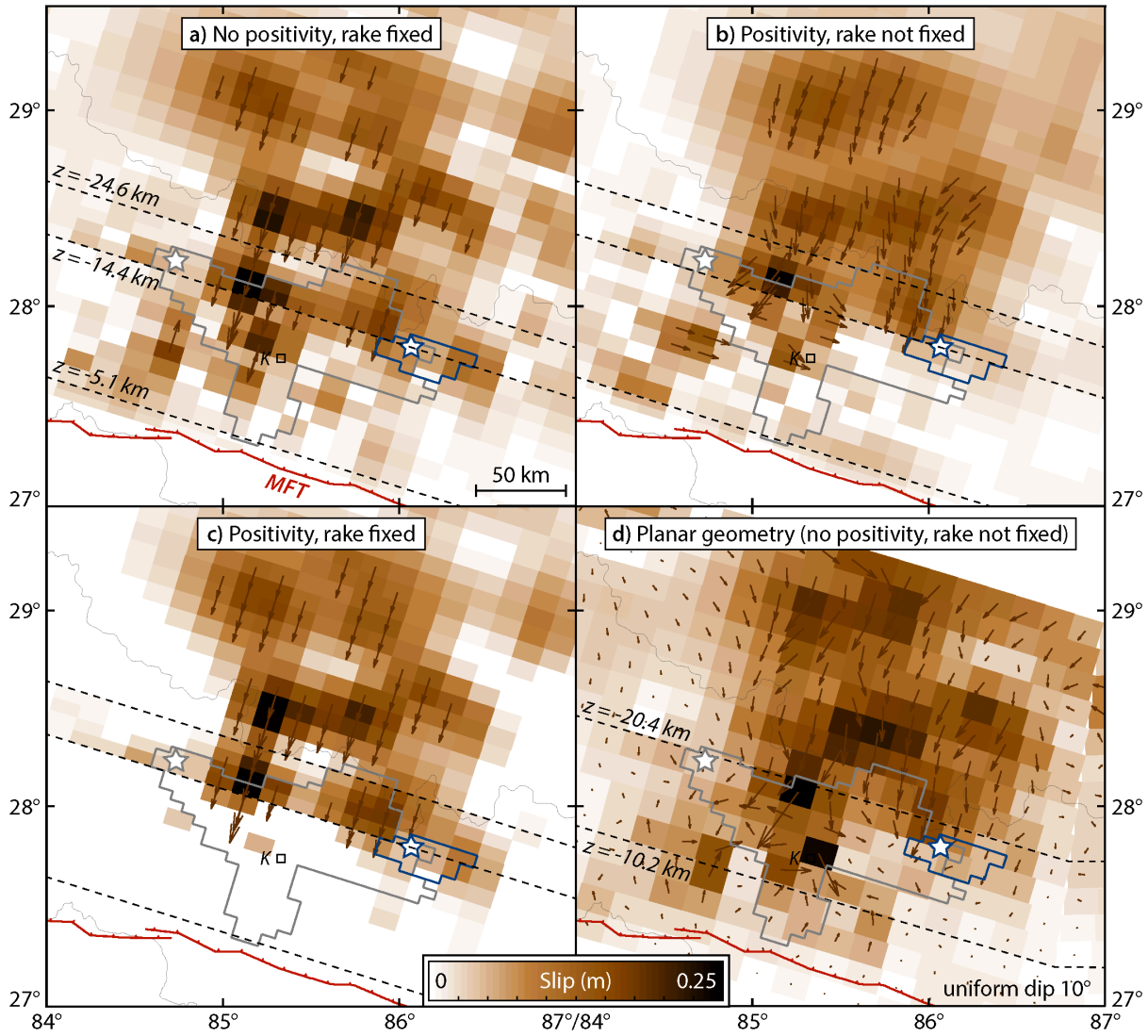

Figure S3. Alternative kinematic inversions for cumulative afterslip. The inversion procedures are the same as in the preferred kinematic model (Figure 8a) except that **a)** the rake is fixed to be pure reverse (but positivity is not enforced); **b)** positivity is enforced (but the rake is not fixed); **c)** the rake is fixed to be pure reverse and positivity is enforced; **d)** a planar dipping MHT geometry is used. Brown arrows: slip vectors for patches with ≥35% of the maximum slip in each model. K: Kathmandu.

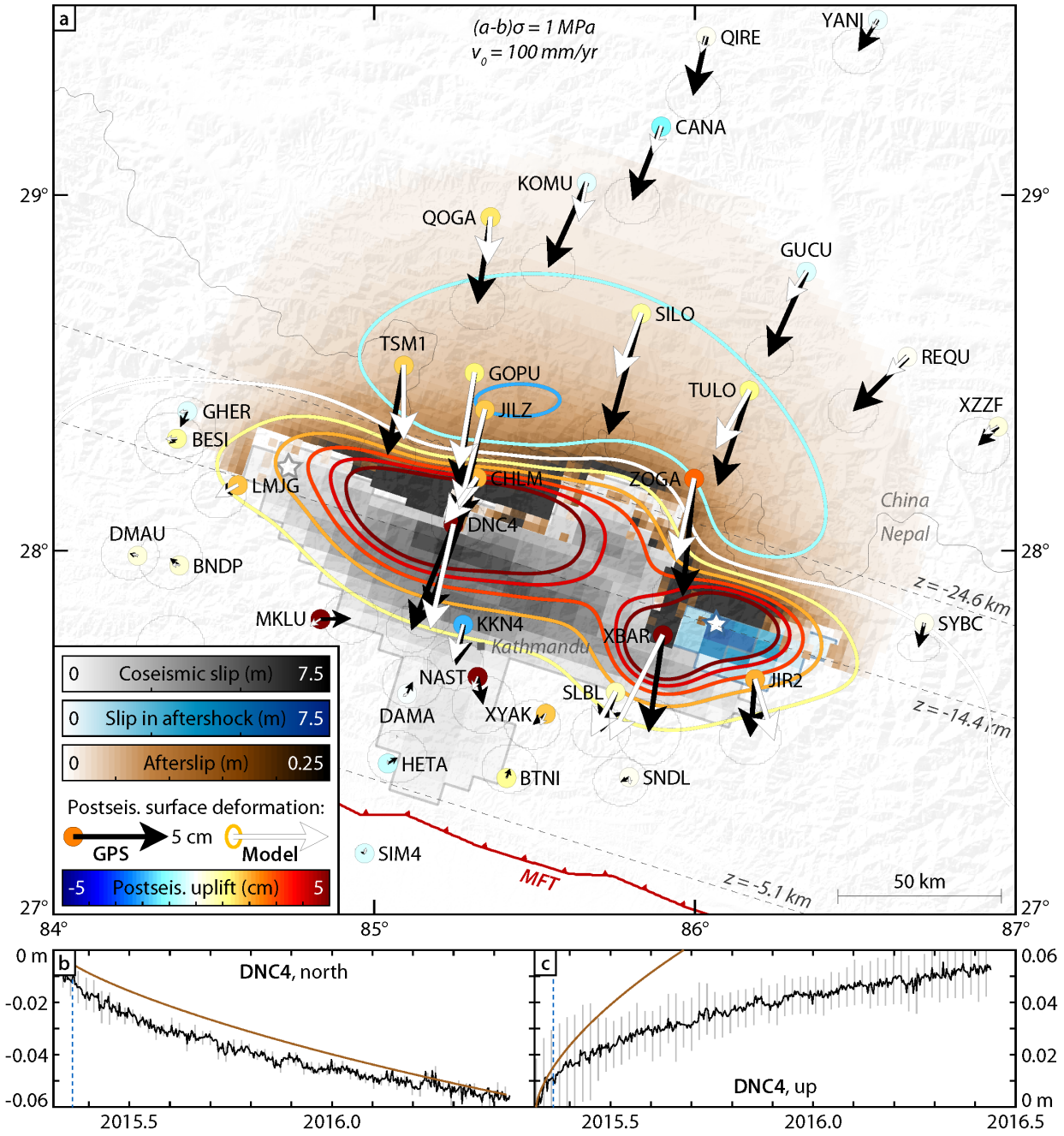

Figure S4. a) Cumulative 1.12-year slip (brown patches) and displacements in forward model of stress-driven afterslip with $(a-b)\sigma$ = 1 MPa and V_0 = 100 mm/yr. Black and white arrows: observed and predicted horizontal displacements. Colored circles and contours: observed and predicted verticals. Gray and blue stars and patches: epicenters and slip in the mainshock and Mw=7.3 aftershock. **b, c)** Observed (black/gray) and predicted displacement timeseries at DNC4.

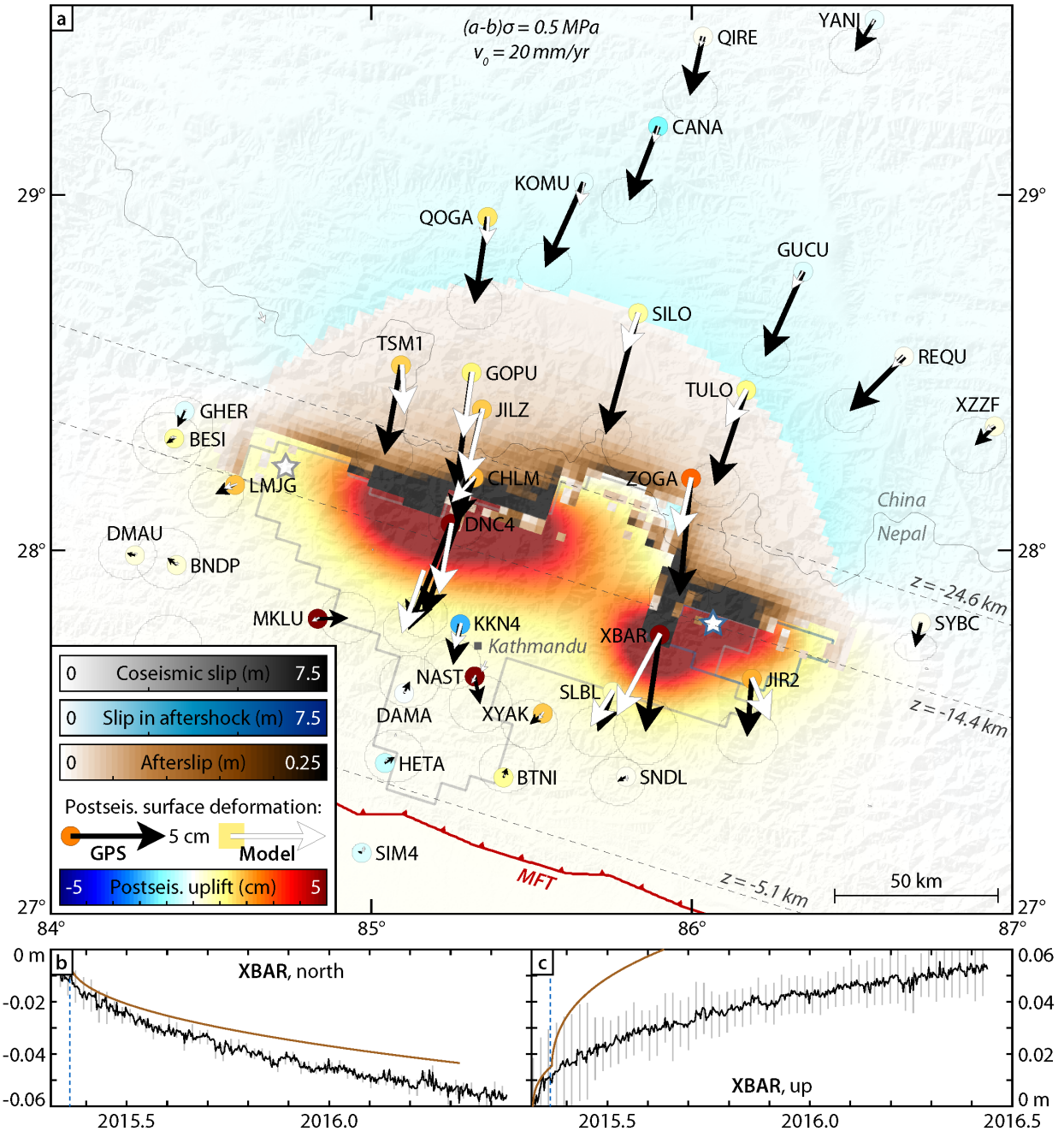

Figure S5. a) Cumulative 1.12-year slip (brown patches) and displacements in forward model of stress-driven afterslip with $(a-b)\sigma$ = 0.5 MPa and V_0 = 20 mm/yr. Black and white arrows: observed and predicted horizontal displacements. Colored circles and shading: observed and predicted verticals. Gray and blue stars and outlines: epicenters and ≥0.25-m-slip areas in the mainshock and Mw=7.3 aftershock. **b, c)** Observed (black/gray) and predicted displacement timeseries at XBAR.

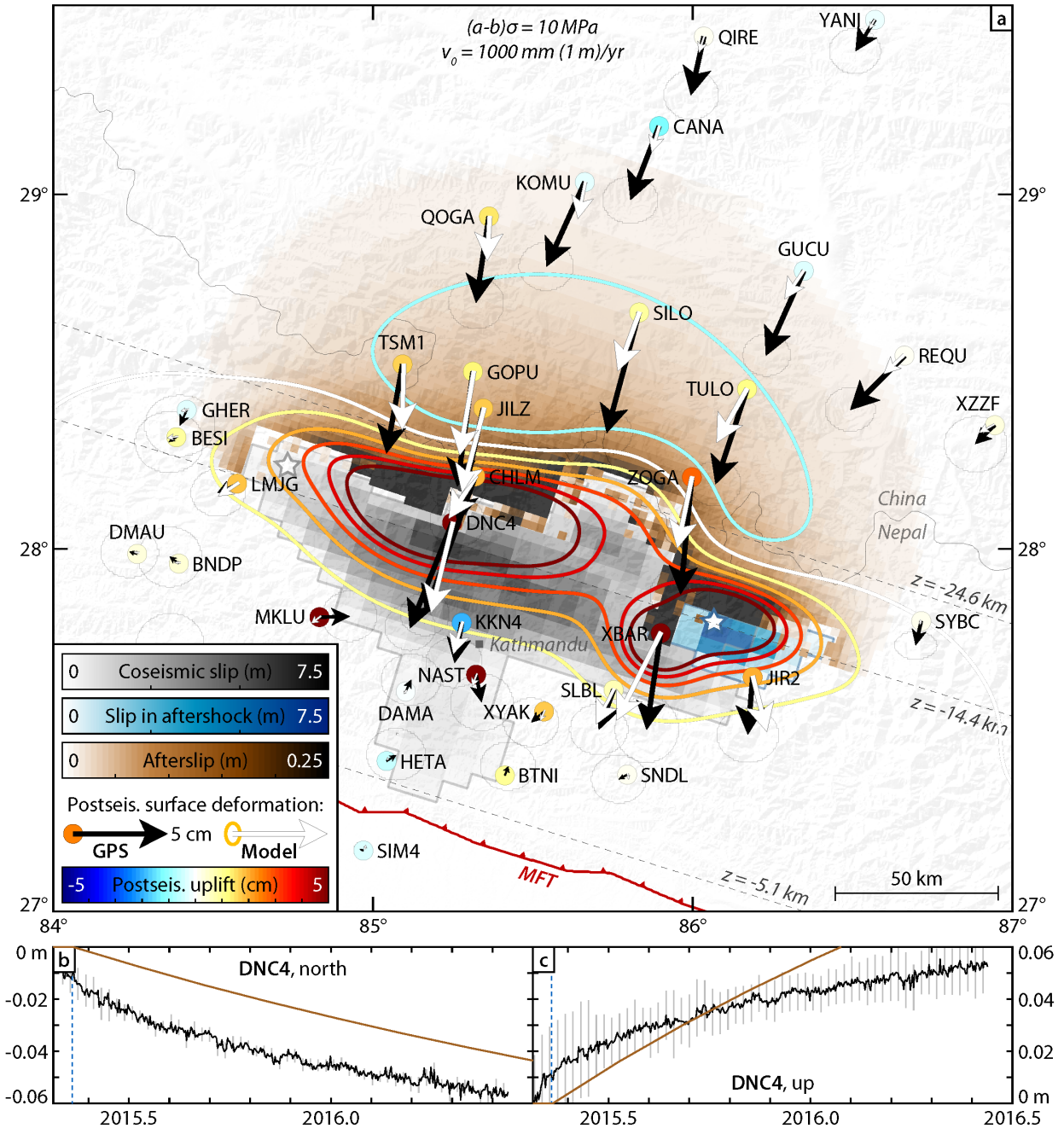

Figure S6. a) Cumulative 1.12-year slip (brown patches) and displacements in forward model of stress-driven afterslip with $(a-b)\sigma$ = 10 MPa and V_0 = 1 m/yr. Black and white arrows: observed and predicted horizontal displacements. Colored circles and contours: observed and predicted verticals. Gray and blue stars and patches: epicenters and slip in the mainshock and Mw=7.3 aftershock. **b, c)** Observed (black/gray) and predicted displacement timeseries at DNC4.

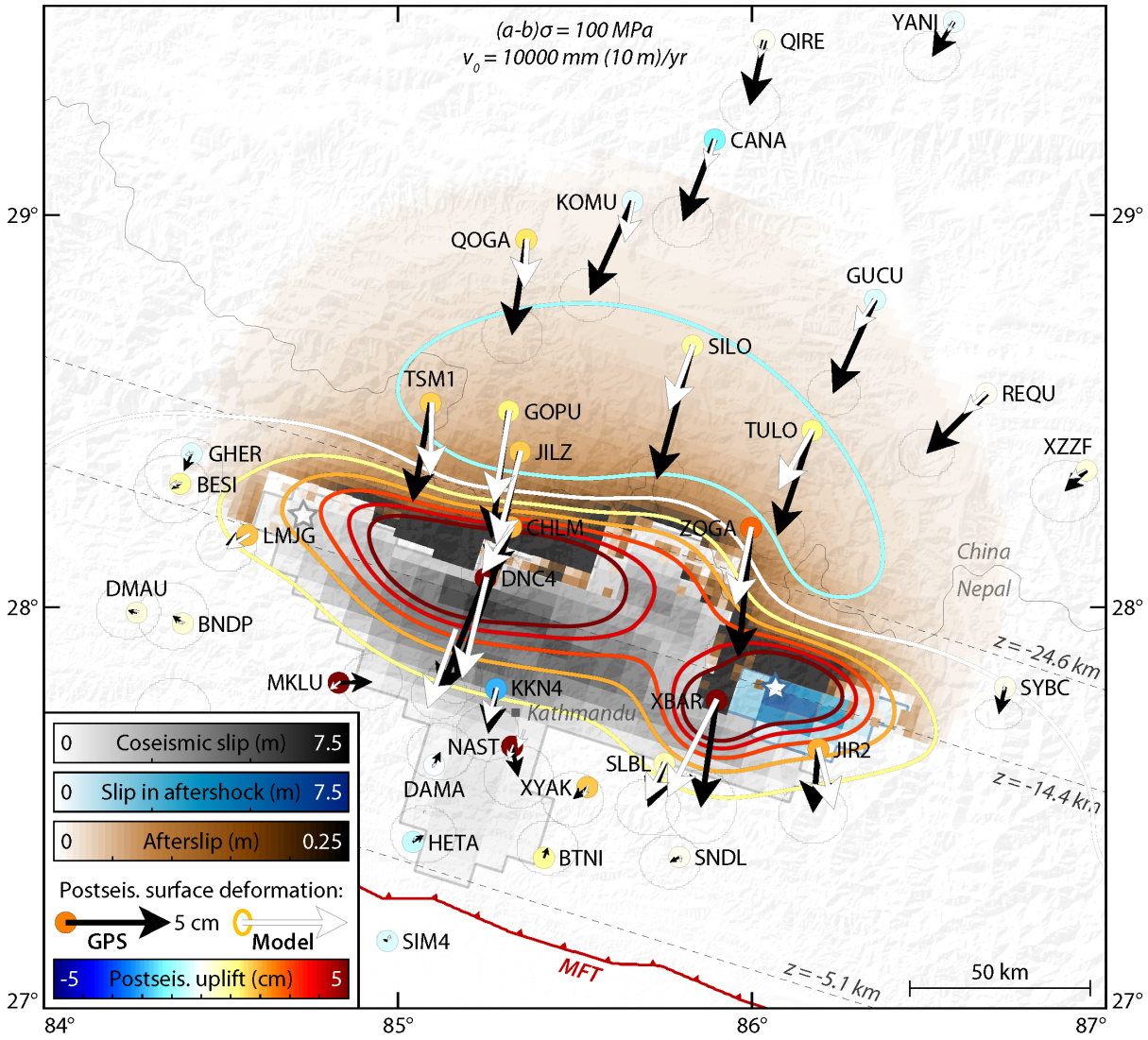

Figure S7. Cumulative 1.12-year slip (brown patches) and displacements in forward model of stress-driven afterslip with $(a-b)\sigma$ = 100 MPa and V_0 = 10 m/yr. Black and white arrows: observed and predicted horizontal displacements. Colored circles and contours: observed and predicted verticals. Gray and blue stars and patches: epicenters and slip in the mainshock and Mw=7.3 aftershock.

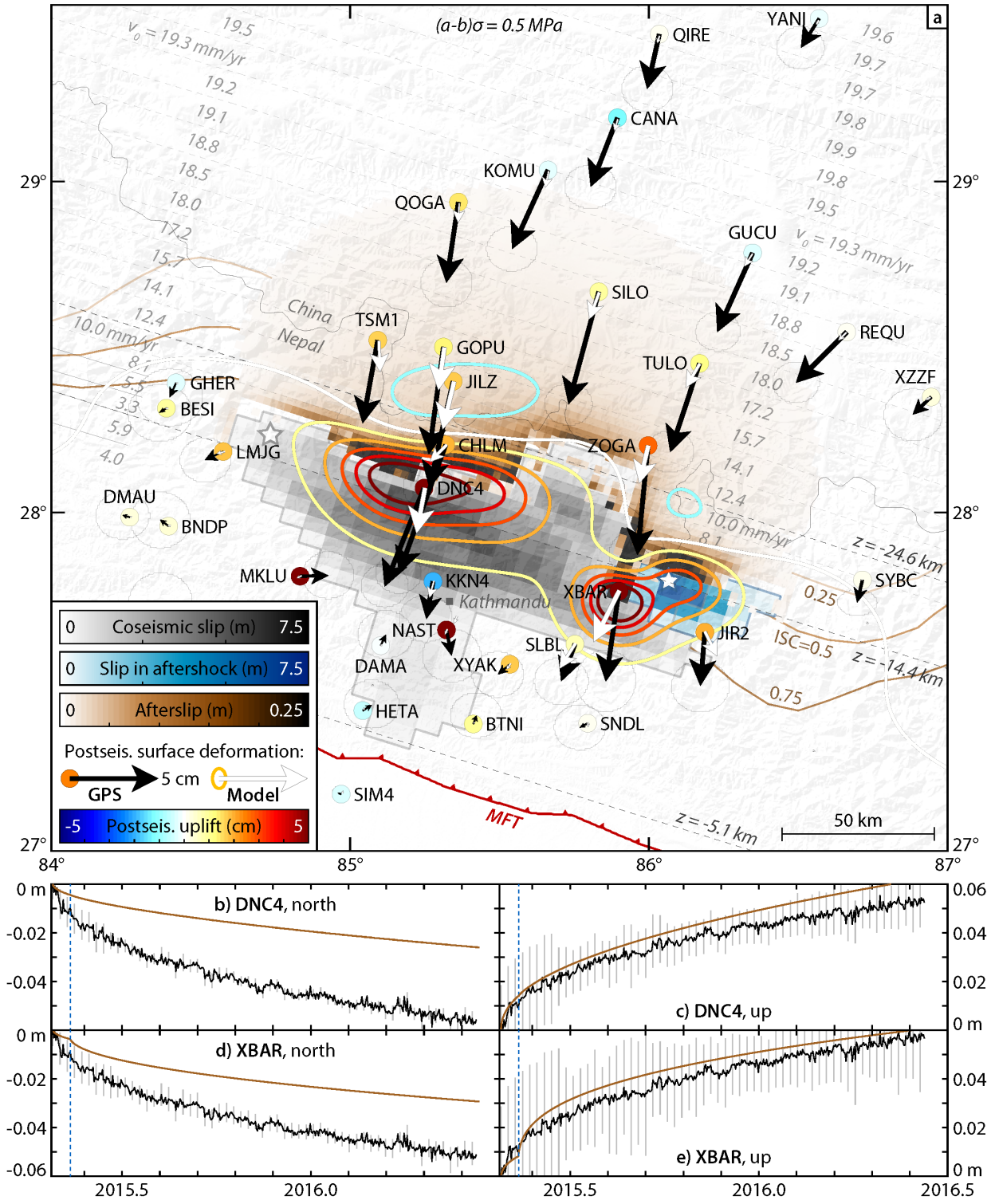

Figure S8. a) Cumulative 1.12-year slip (brown patches) and displacements from stress-driven afterslip with $(a-b)\sigma = 0.5$ MPa and V_0 decreasing downdip (values in gray). Black/white arrows: observed/predicted horizontal motions. Colored circles/contours: observed/predicted verticals. Gray and blue stars and patches: mainshock and Mw=7.3 aftershock. **b-e)** Observed (black/gray) and predicted (brown) displacement timeseries at DNC4 and XBAR.

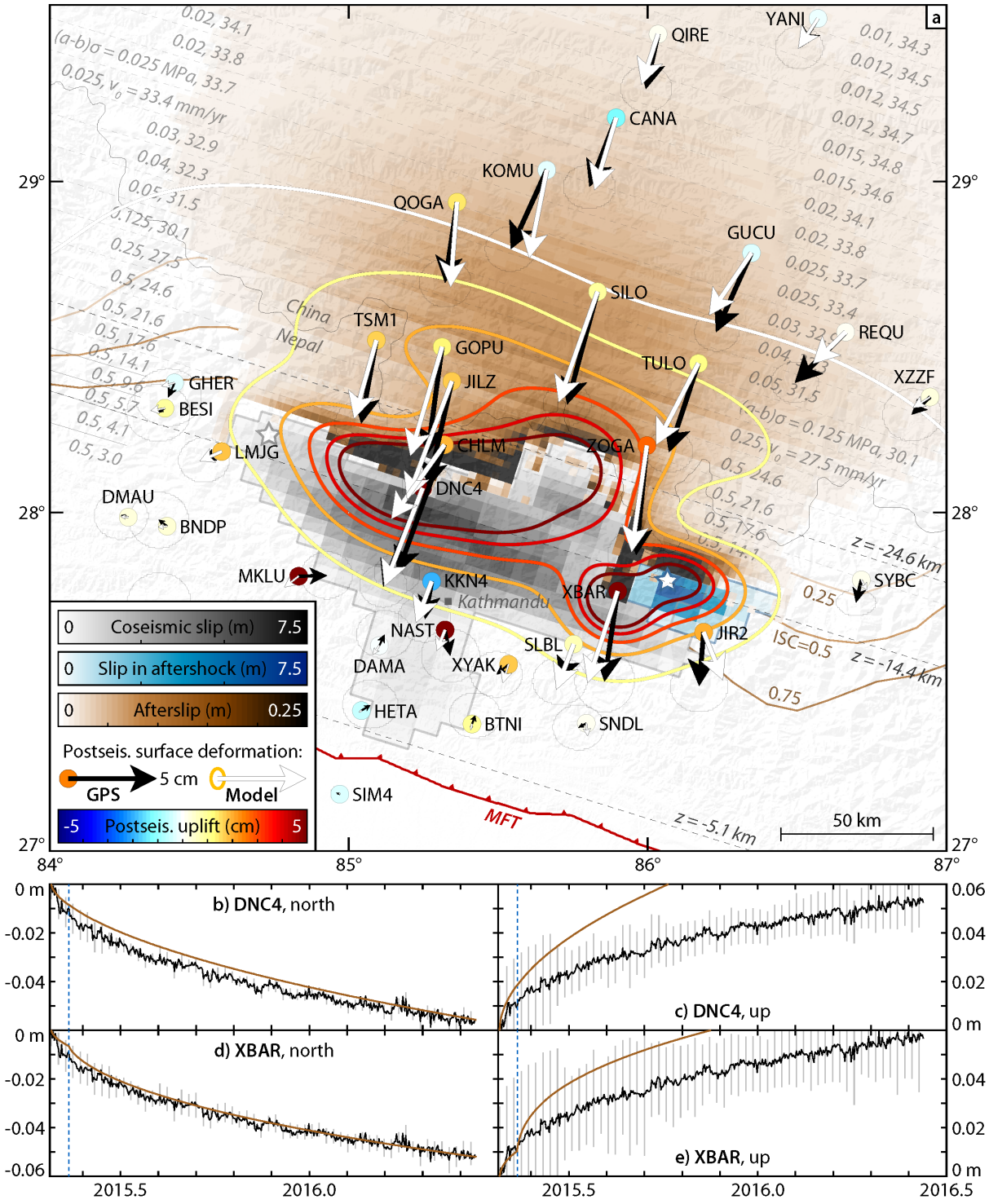

Figure S9. a) Cumulative 1.12-year slip (brown patches) and displacements in stress-driven afterslip model with $(a-b)\sigma$ and V_0 both decreasing downdip (values in gray). Black/white arrows: observed/predicted horizontal motions. Colored circles/contours: observed/predicted verticals. Gray and blue stars and patches: epicenters and slip in mainshock and Mw=7.3 aftershock. **b-e)** Observed (black/gray) and predicted (brown) displacement timeseries at DNC4 and XBAR.

$(a-b)\sigma$	v_0	χ^2/N	VR (%)	Notes
1 MPa, uniform	20 mm/yr, uniform	4.40	32.6%	"Basic forward afterslip model" (Figure 10)
1 MPa, unif.	100 mm/yr, uniform	2.08	51.3%	Figure S4
10 MPa, unif.	1 m/yr, uniform	2.73	51.8%	Figure S6
0.5 MPa	Interseismic creep rate (averaged laterally)	3.70	41.3%	Figure S8
Decreasing northward from 1 MPa to 0.01 MPa	35 mm/yr, uniform	0.79	78.1%	"Maximal forward afterslip model" (Figure 11)
Decreasing northward from 1 MPa to 0.01 MPa	Interseismic creep rate (averaged laterally) x 7/4 (max = 35 mm/yr)	0.79	76.5%	Figure S9

Table S1. Selected forward afterslip models and misfits to the timeseries of the first postseismic IC.